Pulse Radiation from an Insulated Antenna: An Analog of Cherenkov Radiation from a Moving Charged Particle

Thorsten W. Hertel, *Student Member, IEEE,* and Glenn S. Smith, *Fellow, IEEE*

***Abstract*—Cherenkov radiation arises when a charged particle moves with a constant velocity that is greater than the speed of light in the surrounding medium. This radiation has distinctive characteristics. Near the charge, the electric field is most intense along a conical surface with apex at the charge—the Mach cone. In the far field, the radiation occurs predominantly in one direction—at the Cherenkov angle. An insulated antenna consists of a metallic cylindrical conductor covered by a concentric sheath of dielectric. In use, this antenna is embedded in a medium whose permittivity is often much greater than the permittivity of the insulation. When the antenna is excited by a pulse of voltage, a pulse of charge appears to travel along its length. The apparent velocity of this charge is close to the speed of light in the insulation, which, because of the difference in the permittivities, is greater than the speed of light in the surrounding medium. Thus, the radiation from the pulse excited, insulated antenna should be analogous to Cherenkov radiation from the moving charged particle. In this paper, the pulse-excited, traveling-wave insulated linear antenna is accurately analyzed using the finite-difference time-domain (FDTD) method. Results are obtained for the charge on the conductor, the near field, and the far field. These results show the striking similarity of the radiation from this antenna to Cherenkov radiation from the moving charge.**

***Index Terms*—Cherenkov radiation, electromagnetic transient propagation, FDTD, insulated antennas.**

I. Introduction

In the 1930's, the Russian scientists Cherenkov and Vavilov observed visible radiation in experiments with pure liquids under the action of fast electrons [1], [2]. This radiation had distinctive characteristics that could not be explained with any theory of luminescence: fixed polarization, spatial symmetry, and absolute intensity. A full theoretical explanation for the radiation based on classical electromagnetic theory was provided by Frank and Tamm in 1937 [3], [4]. The radiation was caused by charged particles—electrons—moving with a constant velocity v greater than the speed of light $c_n = c/\sqrt{\epsilon_r}$ in the surrounding liquid. Here, ϵ_r is the relative permittivity of the liquid. In 1958, Cherenkov, Frank, and Tamm received the Nobel Prize in Physics for their discoveries. Today, this radiation is called "Cherenkov radiation" or "Cherenkov–Vavilov radiation."

Manuscript received November 3, 1998; revised November 16, 1999. This work was supported in part by the Joint Services Electronics Program under Contract DAAH-04-96-1-0161.

The authors are with the School of Electrical and Computer Engineering, Georgia Institute of Technology, Atlanta, GA 30332-0250 USA.

Publisher Item Identifier S 0018-926X(00)01660-4.

An insulated antenna consists of a metallic, cylindrical conductor covered by a concentric sheath of dielectric with relative permittivity ϵ_{ri} [5]. Insulated antennas are most effective when they are used in a material whose electrical properties are quite different from those of the insulation; that is, either the relative permittivity ϵ_{re} or the conductivity σ_e of the external medium is much greater than that of the insulation. All previous analyses of insulated antennas have been for time-harmonic excitation [5], [6]. The characteristics of the insulated antenna are then very different from those of a similar bare antenna whenever $|k_e/k_i|^2 \gg 1$, where k_e and k_i are the complex wavenumbers in the external medium and the insulation, respectively.

Consider the case where both the insulation and the external medium have negligible loss, and the ratio of permittivities is large; that is, $\epsilon_{re}/\epsilon_{ri} \gg 1$. When the antenna is excited by a pulse of voltage, a pulse of charge appears to travel along its length. The apparent velocity of this charge is close to the speed of light in the insulation $c_{ni} = c/\sqrt{\epsilon_{ri}}$, which, because of the difference in the permittivities, is greater than the speed of light in the surrounding medium $c_{ne} = c/\sqrt{\epsilon_{re}}$. Thus, the radiation from the pulse-excited insulated antenna should be analogous to Cherenkov radiation from a moving charged particle [2].

In this paper, the pulse-excited, traveling-wave, insulated linear antenna is accurately analyzed using the finite-difference time-domain (FDTD) method. This is an insulated linear antenna with a source at one end and a termination at the opposite end. Both the source and the termination are constructed to produce very low reflection. The pulse of charge then appears to move at approximately constant velocity over a path of finite length in the external medium. Results are obtained for the charge on the conductor, the near field, and the far field. Detailed plots show the striking similarity of the radiation from this antenna to Cherenkov radiation from the moving charge.

II. Cherenkov Radiation from a Moving Charge

The general characteristics of Cherenkov radiation for a point charge moving with constant velocity $\vec{v}$ are shown schematically in Fig. 1. Near the charge, the field is confined to the interior of a cone, the Mach cone, with its axis along the path of the charge and its apex at the charge (the shaded region in the figure). The obtuse angle between the side of the cone and the velocity vector is $\theta_c = \pi/2 + \chi_c$. The field is most intense on the surface of this cone, where it is also tangential to this surface. The Poynting vector $\vec{\mathcal{S}}$ is normal to this surface; thus, $\vec{\mathcal{S}}$ is at the angle χ_c to

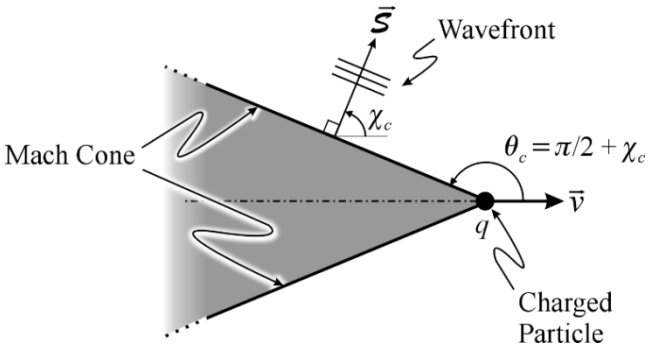

Fig. 1. Schematic drawing used to describe Cherenkov radiation.

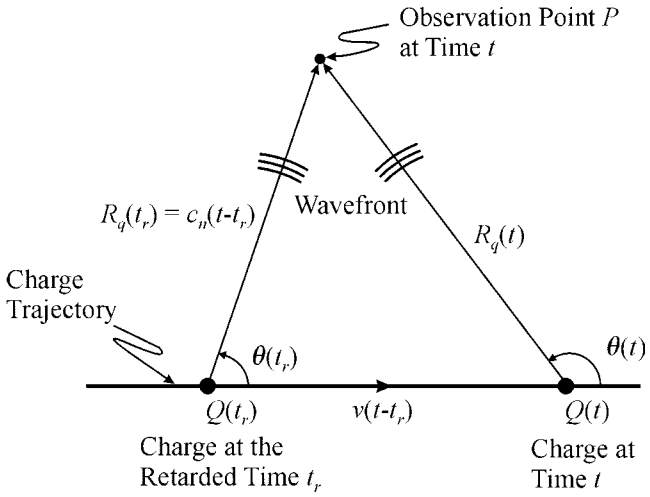

Fig. 2. Geometry for determining the retarded times.

the velocity vector. When the charge travels over a path of finite length, the radiation (far field) is most intense at the Cherenkov angle χ_c.

The existence of the Mach cone can be explained with a simple argument based on the retarded time. Consider the geometry shown in Fig. 2. The field is being observed at point P at the current time t. The current position of the charge is indicated by $Q(t)$ on the right-hand side of the figure. The field at P was radiated by the charge at the earlier, retarded time t_r when it was at the position $Q(t_r)$. A straightforward analysis obtains the following expression for the retarded time [2]:

$$t_r[R_q(t), \theta(t)] = t - \frac{R_q(t)}{c_n}\frac{1}{\beta_n^2 - 1} \cdot \left[-\beta_n \cos\theta(t) \pm \sqrt{1 - \beta_n^2 \sin^2\theta(t)}\right] \quad (1)$$

with

$$\beta_n = \frac{v}{c_n} = \frac{\sqrt{\epsilon_r}\, v}{c} > 1. \quad (2)$$

For angles in the range $0 \le \theta(t) < \theta_c$, where

$$\theta_c = \pi - \sin^{-1}(1/\beta_n), \qquad \pi/2 < \theta_c < \pi \quad (3)$$

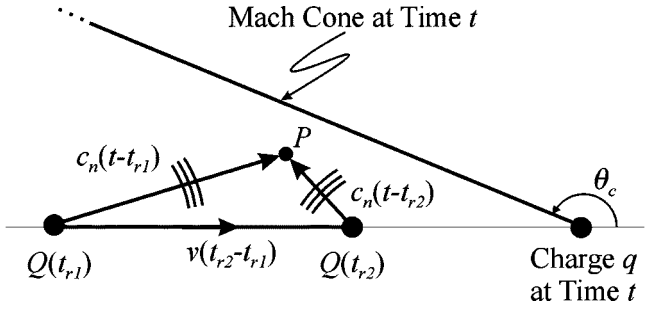

Fig. 3. Explanation for the Mach cone.

or

$$\chi_c = \cos^{-1}(1/\beta_n) = \cos^{-1}\left(\frac{c_n}{v}\right) \quad (4)$$

the retarded times given by (1) are either complex numbers or violate causality. This explains the absence of field outside the Mach cone. For angles within the range $\theta_c \le \theta(t) \le \pi$, that is, within the Mach cone, there are two retarded times indicated by the $\pm$ sign in (1).

Recall that for a charge moving in free-space ($v < c$), there is only one retarded time associated with each position P at time t. The fact that there are now two retarded times is a consequence of the charge traveling with a velocity greater than the speed of light in the surrounding medium ($v > c_n = c/\sqrt{\epsilon_r}$) and it is easily explained by a simple geometric argument based on Fig. 3.

At the retarded time $t_{r1} < t_{r2}$, the charge is at position $Q(t_{r1})$ from where it radiates a spherical wavefront. This wavefront arrives at point P after the time interval $\tau_1 = t - t_{r1} = \overline{Q(t_{r1})P}/c_n$. In the meantime, the charge continues to move along its trajectory, reaching the position $Q(t_{r2})$ after the time interval $\tau_q = t_{r2} - t_{r1} = \overline{Q(t_{r1})Q(t_{r2})}/v$. The spherical wavefront radiated by the charge at position $Q(t_{r2})$ arrives at point P after the time interval $\tau_2 = t - t_{r2} = \overline{Q(t_{r2})P}/c_n$. From simple geometry, it is clear that the distances over which the radiation and charge travel must satisfy the inequality

$$\overline{Q(t_{r1})Q(t_{r2})} + \overline{Q(t_{r2})P} > \overline{Q(t_{r1})P}. \quad (5)$$

However, the time intervals corresponding to these distances can be equal; that is

$$\tau_q + \tau_2 = \tau_1 \quad (6)$$

or

$$\overline{Q(t_{r1})Q(t_{r2})}/v + \overline{Q(t_{r2})P}/c_n = \overline{Q(t_{r1})P}/c_n. \quad (7)$$

Therefore, radiation originating at the particle at two different retarded times (t_{r1} and t_{r2}) can arrive at the point P at the same time t. This result is solely a consequence of the particle traveling with a velocity v faster than the speed of light in the surrounding medium c_n.

The discussion presented above is for a moving point charge. There are more realistic models that assume a charge of finite size or a bunch of charges. For one such model, the volume

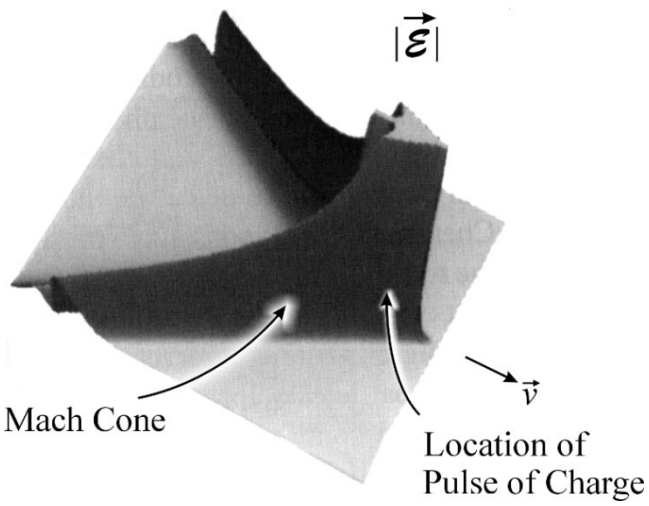

Fig. 4. Magnitude of the electric field near a moving particle that is a Gaussian pulse of charge $\beta_n = 2.0$ from [7].

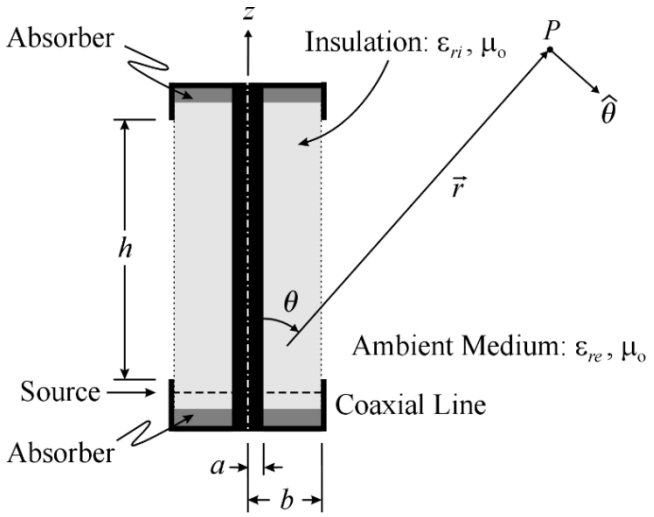

Fig. 5. Model of the insulated traveling-wave antenna.

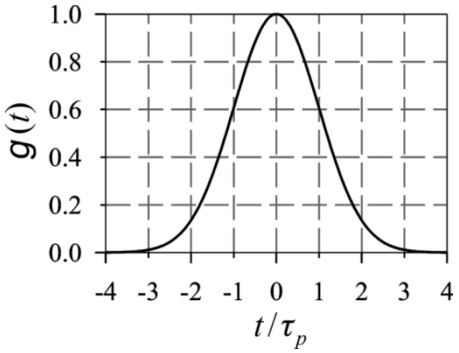

Fig. 6. Gaussian function versus normalized time.

density of charge is a Gaussian function along the path of the particle (z axis)

$$\rho(\vec{r}, t) = \frac{q}{\sqrt{2\pi}\, s_p}\, \delta(x)\delta(y) e^{-0.5(z-vt)^2/s_p^2}. \tag{8}$$

The accompanying volume density of current is

$$\vec{\mathcal{J}}(\vec{r}, t) = \frac{qv}{\sqrt{2\pi}\, s_p}\, \delta(x)\delta(y) e^{-0.5(z-vt)^2/s_p^2} \hat{z}. \tag{9}$$

In these expressions, the parameter s_p determines the spatial extent of the distribution. Analytic expressions have been obtained for the electromagnetic field of this distribution [2], [7]. Fig. 4 shows the magnitude of the electric field $|\vec{\mathcal{E}}|$ in a region surrounding the charge. Notice that the field is most intense along the side of the Mach cone and is negligible outside of the Mach cone.

III. Insulated Traveling-Wave Antenna

In this section, a model is developed for an insulated antenna that launches a pulsed signal over a finite length. This antenna is shown in Fig. 5. At the bottom end, it is driven by a short section of coaxial line containing a matched source, and at the top end, it is terminated with a short section of coaxial line containing a matched load. The height h is measured between the openings of the coaxial lines, and the radius of the insulation b is identical to the inner radius of the outer conductor of the coaxial lines. The radius of the perfectly conducting center conductor is a. Both the insulation and the ambient medium are assumed to be lossless and nonmagnetic. The relative permittivity for the insulation is ϵ_{ri}, and the relative permittivity for the external medium is ϵ_{re}. The antenna is driven by an incident signal injected at the source plane. With this antenna model, a wave launched at the drive point propagates over a finite length h until it is almost totally absorbed at the opposite end. The antenna is rotationally symmetric, thus any field point P outside the antenna is characterized only by the angle θ measured from the z axis and the radius r measured from the origin, which is at the drive point.

The time-domain analysis of this antenna is performed with an incident Gaussian voltage pulse of the form

$$\mathcal{V}(t) = V_\circ\, e^{-0.5(t/\tau_p)^2} \tag{10}$$

where τ_p is the characteristic time of the pulse. In Fig. 6, the temporal dependence of the normalized Gaussian function $g(t) = \mathcal{V}(t)/V_\circ$ is shown. For future reference, the pulse width is defined to be approximately $4.3\tau_p$, which is the time interval between the points at which the amplitude is ten percent of its maximum value.

Arguments similar to those used with Fig. 3 for the charged particle can be applied to predict the far-field characteristics of the insulated traveling-wave antenna. Notice that a time-domain investigation is especially useful for explaining the phenomenon of Cherenkov radiation, where delay and arrival times play significant roles. The analogous Cherenkov angle χ_c for the insulated linear antenna can be determined easily with the following simple argument. Recall first that under the assumption that the permittivity of the external medium is greater than that of the internal medium, the pulse of charge on the antenna appears to travel at a speed c_{ni} greater than the speed of light in the external medium c_{ne}. Maximum radiation occurs when the radiation from the drive point and the opposite end coincide in time at the far-field observation point P, as illustrated in Fig. 7. Since the path that includes the antenna height h and the distance R is spatially longer than the distance r, for constructive

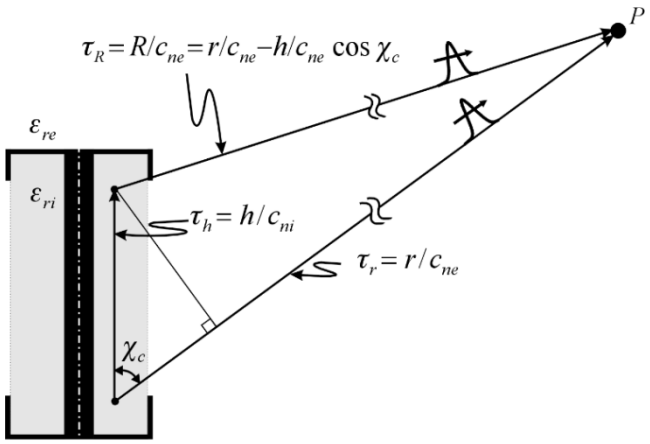

Fig. 7. Schematic drawing used to describe the radiation from the insulated traveling-wave antenna.

interference the wave in the insulation must travel with a speed greater than that in the external medium. This is satisfied for the above mentioned properties, i.e., $c_{ni} > c_{ne}$. Simple geometry and matching of the retardation times ($\tau_h + \tau_R = \tau_r$) result in the equation for the analogous Cherenkov angle

$$\chi_c = \cos^{-1}\left(\frac{c_{ne}}{c_{ni}}\right) = \cos^{-1}\sqrt{\frac{\epsilon_{ri}}{\epsilon_{re}}}. \tag{11}$$

Notice that this angle is exactly the same as found for the Cherenkov angle of the charged particle (4) if the speed of light in the internal medium c_{ni} is replaced by the velocity of the charge v.

The results to be presented in the following section were obtained using the finite-difference time-domain (FDTD) method. This numerical scheme as applied to this antenna is described in more detail in [8]. Due to the antenna's rotational symmetry, the analysis is carried out with a discretization in two dimensions ρ and z. In the FDTD analysis, a "one-way" injector is placed at the source plane within the coaxial line [8]–[10]. This launches the incident pulse in one direction—up the antenna. The reflected pulse is monitored at a point below the one-way injector. The discretized domain is truncated near the antenna with the cylindrical, perfectly-matched layer (PML), absorbing boundary condition [11]. Its uniaxial anisotropic material absorbs the outgoing electromagnetic energy with negligible reflection; typically, the reflected field is less than 0.1% of the incident field. Since the PML is truncating the FDTD lattice close to the antenna, only the near field is directly computed. To obtain the radiated field (far field) a near-field to far-field transformation is used. This transformation is based on Huygens' principle, and the radiated field is determined from the tangential components of the field on a cylindrical surface close to the antenna using a convolution [8], [10].

IV. Numerical Results

For the insulated linear antennas used in this study, the ratio of the permittivity of the external medium to that of the insulation is $\epsilon_{re}/\epsilon_{ri} = 6.83$. The analogous Cherenkov angle (11) is then $\chi_c = 67.5°$, which is a convenient value for use with graphical results. The radius of the insulation relative to that of the center conductor is $b/a = 14$. The coaxial sections at the top and bottom of the antenna are b and $1.5b$ long, respectively, and both are formed from perfect conductors of thickness a.

TABLE I
Parameters for the Three Antennas

	short	medium	long
h/a	155	310	620
b/a	14	14	14
τ_p/τ_{ai}	$1.07 \cdot 10^{-1}$	$5.37 \cdot 10^{-2}$	$2.68 \cdot 10^{-2}$
$\tau_{ai}/4.3\tau_p$	2.2	4.3	8.7

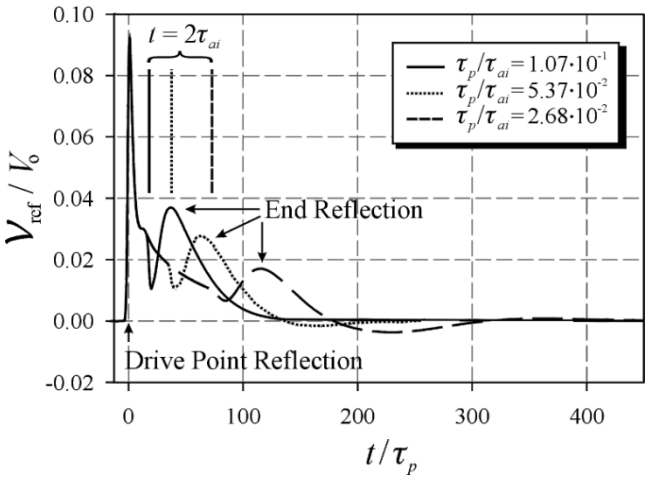

Fig. 8. Reflected voltage within the lower coaxial line as a function of normalized time for the three different antenna lengths.

Three different lengths for the antenna are considered: $h/a = 155$, 310, and 620. The characteristic time for the Gaussian voltage pulse τ_p is chosen to make $\tau_p/\tau_{ai} = 1.07 \cdot 10^{-1}$, $5.37 \cdot 10^{-2}$, and $2.68 \cdot 10^{-2}$, where $\tau_{ai} = h/c_{ni}$ is the time for light to travel the length of the antenna in the insulation. These three lengths correspond to roughly 2.2, 4.3, and 8.7 pulses fitting along the length of the antenna. The parameters for these three antennas are summarized in Table I.

A. Reflected Voltage

The terminations in the coaxial lines at the two ends of the antenna should completely absorb any incoming TEM waves. However, since the waves along the insulated section of the antenna are not purely TEM, there are some small reflections. Fig. 8 shows the normalized reflected voltage $\mathcal{V}_{\rm ref}/V_{\rm o}$ measured in the lower coaxial line just below the one-way injector. Results are shown for the three lengths of the antenna versus normalized time, t/τ_p. In each case, there is a sharp peak near $t/\tau_p = 0$ whose amplitude is about 0.09. This reflection arises at the transition between the lower coaxial line and the insulated antenna, that is, where the outer conductor of the coaxial line stops. A second smaller and much broader peak occurs at about $t/\tau_p = 2\tau_{ai}/\tau_p$ (the round-trip time on the antenna). This is the reflection from the top end of the antenna. The longer the antenna, the lower is this reflection; however, in all three cases it is less than 0.04.

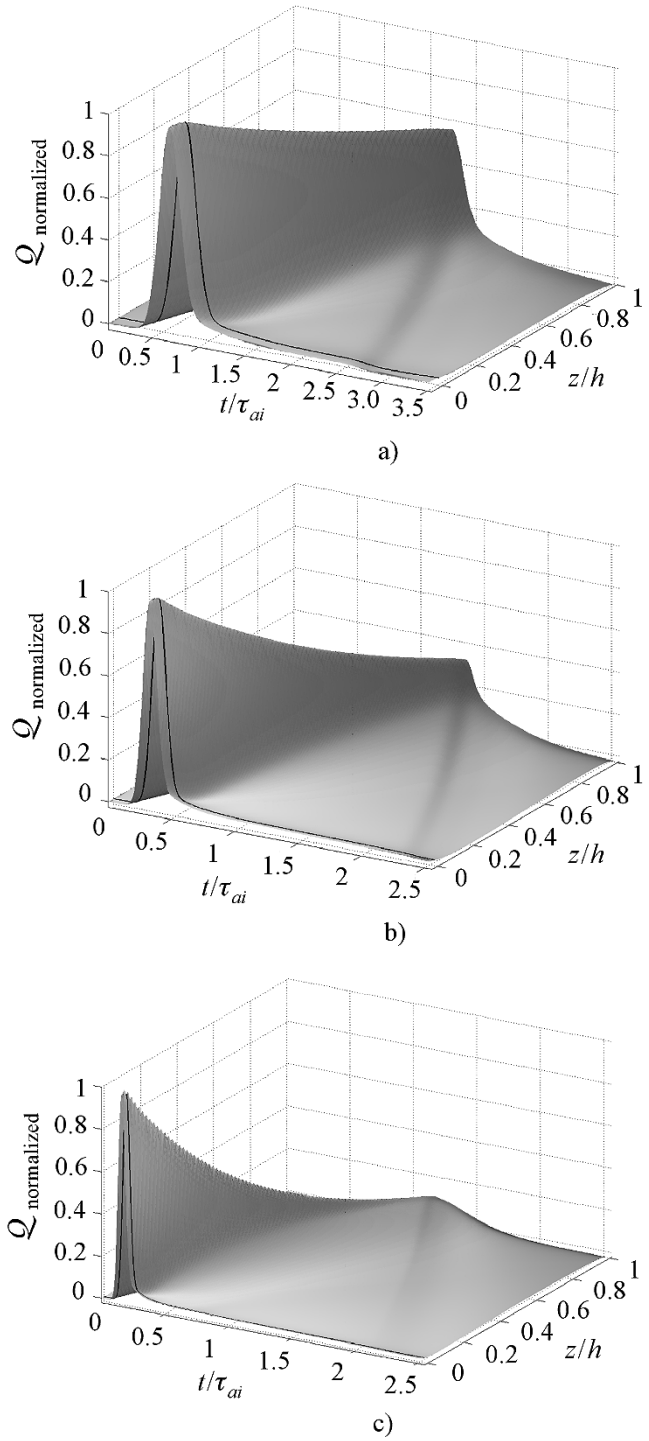

Fig. 9. Charge on the antenna conductor as a function of time and space for antennas of length. (a) $h/a = 155$. (b) $h/a = 310$. (c) $h/a = 620$.

B. Charge Distribution

The normalized charge density on the center conductor of the antenna is shown as a function of the normalized time t/τ_{ai} and the normalized position z/h in Fig. 9. The thick black line on each plot indicates the location of the end of the outer conductor of the lower coaxial line. These graphs show some interesting features. First, the pulse of charge, as expected, appears to travel up the antenna roughly at the speed of light in the insulation; the time for the pulse to travel from the source to the top end of the antenna is roughly $t/\tau_{ai} = 1$ in all three cases. Second, the pulse is attenuated as it travels along the antenna. For the shortest antenna, Fig. 9(a), the amplitude of the pulse is reduced by about a factor of two by the time it reaches the top end, while for the longest antenna, Fig. 9(c), it is reduced by nearly a factor of ten. Third, the reflection of the charge from the top end of the antenna is very small.

C. Near Field

Figs. 10 and 11 are grayscale plots of the magnitude of the electric field near the antenna with length $h/a = 310$ ($t_p/\tau_{ai} = 5.37 \cdot 10^{-2}$). The three plots in Fig. 10 are for different times: (a) when the pulse of charge is halfway up the antenna ($t/\tau_{ai} = 0.5$); (b) when the pulse of charge has just reached the top ($t/\tau_{ai} = 1.0$); and (c) when the reflected pulse has traveled halfway down the antenna ($t/\tau_{ai} = 1.5$). In all of these plots, only the right-hand side of the antenna is shown, and the field within the insulation has been reduced by a factor of 37.

A conical surface, which is similar to the Mach cone shown in Fig. 4 for the charged particle, is clearly seen. For the first two times, Figs. 10(a) and (b), the apex of the cone is at the center of the pulse of charge. The angle between the base and side of the cone, shown in Fig. 10(c), is measured to be 67.5°, which matches the analogous Cherenkov angle χ_c calculated from the relative permittivities of the insulation and the external medium (11).

Fig. 11 shows the details of the electric field near the antenna ($h/a = 310$) at the later time $t/\tau_{ai} = 3.0$. A conical wavefront, which makes the angle χ_c with the axis of the antenna, has been established and is propagating away from the antenna. The ends of the wavefront are spherical surfaces W_1 and W_2 centered on the two ends of the antenna. The small graphs on the right of Fig. 11 show the two components of the electric field at five points along the conical wavefront. Notice that the tangential component of the field $\mathcal{E}_t$ is much larger than the normal component $\mathcal{E}_n$. This finding is in close agreement with what is observed for Cherenkov radiation from a moving charged particle [2], [7].

Notice that the field in Fig. 11 is very intense around the two ends of the antenna. This is a result of charge accumulation at these points. When the positive pulse of charge leaves the source, it leaves behind an equal amount of negative charge in the bottom coaxial line, and when the positive pulse of charge enters the termination at the top of the antenna, it deposits charge in the coaxial line.

D. Far Field

The radiated or far fields for the three antennas are shown in Fig. 12. Each of the graphs (a, b, and c) presents the following information. Consider a large spherical surface of radius $r_\circ$ centered at the lower end of the antenna. Observers are stationed at the polar angles $\theta = 0°, 22.5°, 45°, \cdots$ on the surface of this sphere. Each observer measures the electric field as a function of time, and the eight plots in each of the graphs show these measured fields. The field $\mathcal{E}_\theta^r$ is graphed positive in the clockwise direction as the arrow at the angle $45°$ indicates.

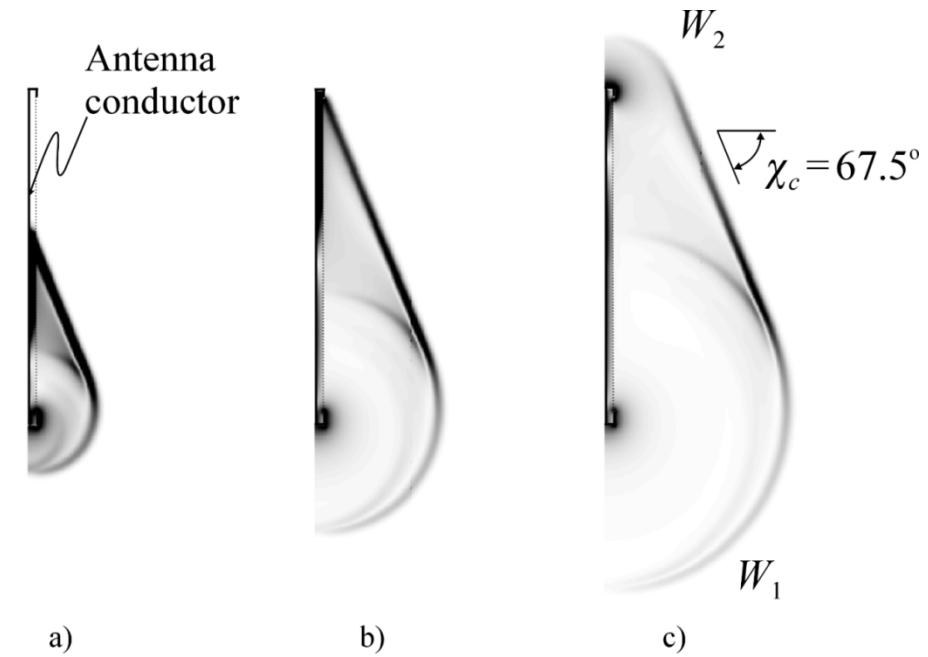

Fig. 10. Grayscale plots showing the magnitude of the electric field near the antenna with $h/a = 310$ for three different times. (a) $t/\tau_{ai} = 0.5$. (b) $t/\tau_{ai} = 1.0$. (c) $t/\tau_{ai} = 1.5$. Only the right-hand side of the antenna is shown.

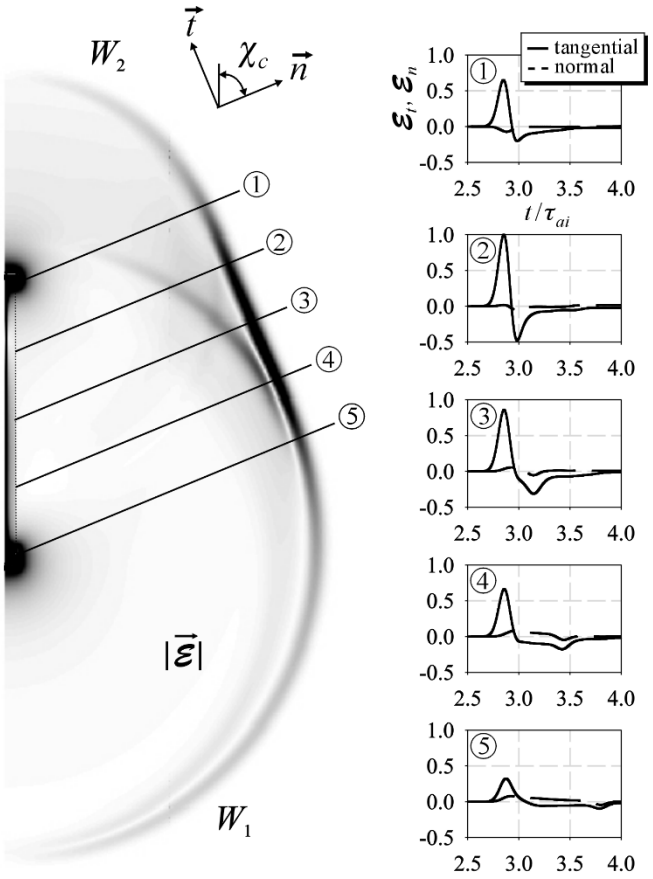

Fig. 11. Grayscale plot showing the magnitude of the electric field near the antenna with $h/a = 310$ for the time $t/\tau_{ai} = 3.0$. Small figures on the right show the electric field components normal and tangential to the surface of the Mach cone.

The dashed curves marked W_1 and W_2 connect the times of arrival for wavefronts that originate at the lower end and upper end of the antenna, respectively. The curve for W_1 is a circle; for all of the observers, the radiation from the bottom end arrives at the same time

$$t_1/\tau_{ai} \approx \frac{c_{ni}}{c_{ne}} \frac{r_\circ}{h} = \sqrt{\frac{\epsilon_{re}}{\epsilon_{ri}}} \frac{r_\circ}{h}. \tag{12}$$

This is a consequence of the spherical surface being centered at the bottom end of the antenna. The curve for W_2 is not a circle; the time of arrival for W_2 relative to W_1 changes with the angle of observation

$$t_2/\tau_{ai} \approx \sqrt{\frac{\epsilon_{re}}{\epsilon_{ri}}} \left(\frac{r_\circ}{h} - \cos\theta\right) + 1 \tag{13}$$

or

$$t_2/\tau_{ai} - t_1/\tau_{ai} \approx 1 - \sqrt{\frac{\epsilon_{re}}{\epsilon_{ri}}} \cos\theta = 1 - \frac{\cos\theta}{\cos\chi_c}. \tag{14}$$

The two wavefronts W_1 and W_2 cross at the analogous Cherenkov angle $\theta = \chi_c = 67.5^\circ$. For angles $\theta > \chi_c$, W_1 arrives before W_2. However, for angles $\theta < \chi_c$, W_2 arrives before W_1, even though the signal for W_2 travels over a longer path than the signal for W_1. This is a consequence of the speed of light in the insulation being greater than the speed of light in the external medium.

Notice from the results in Fig. 12 that the pulse of radiation is largest at the analogous Cherenkov angle χ_c. This finding is again in close agreement with what is observed for Cherenkov radiation from a moving charged particle [2], [7]. Also, notice that the amplitude of the radiation at the analogous Cherenkov

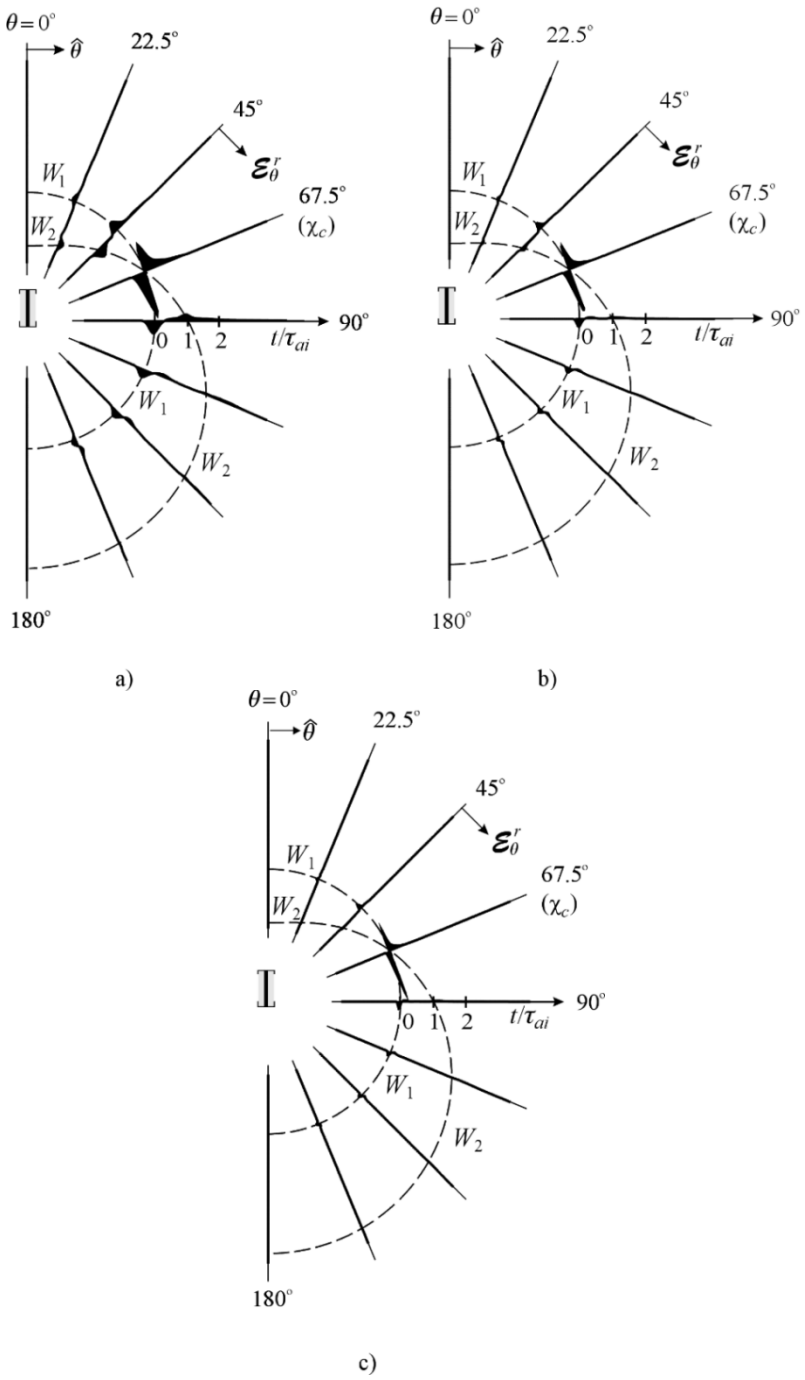

Fig. 12. Radiated electric field for three lengths of the insulated, traveling-wave antenna. (a) $h/a = 155$. (b) $h/a = 310$. (c) $h/a = 620$.

angle increases relative to the radiation at other angles as the length of the antenna is increased. This observation is shown quantitatively in Fig. 13, where the ratio of the maximum electric field at $\theta = \chi_c$ to the maximum electric field at $\theta = 90°$, that is

$$\frac{\max |\mathcal{E}_\theta^r(\theta = \chi_c)|}{\max |\mathcal{E}_\theta^r(\theta = 90°)|}$$

is plotted (line with solid dots) as a function of the normalized length of the antenna for antennas up to about twelve pulse widths long ($\tau_{ai}/\tau_p = 50$).

Results for this ratio can also be obtained from a simple theory [2], [8]. When the charge/current distribution along the antenna is assumed to be a decaying exponential of the form $e^{-\alpha z}$, this ratio can be determined analytically

$$\frac{\max |\mathcal{E}_\theta^r(\theta = \chi_c)|}{\max |\mathcal{E}_\theta^r(\theta = 90°)|} = \sqrt{1 - \left(\frac{c_{ne}}{c_{ni}}\right)^2}\, e^{-1/2} \cdot \frac{1 - e^{-\alpha c_{ni}\tau_p \cdot \tau_{ai}/\tau_p}}{\alpha c_{ni}\tau_p}. \quad (15)$$

For $\alpha c_{ni}\tau_p = 0$ (no attenuation, dashed line on the graph), the ratio is a linear function of the antenna length. For the value

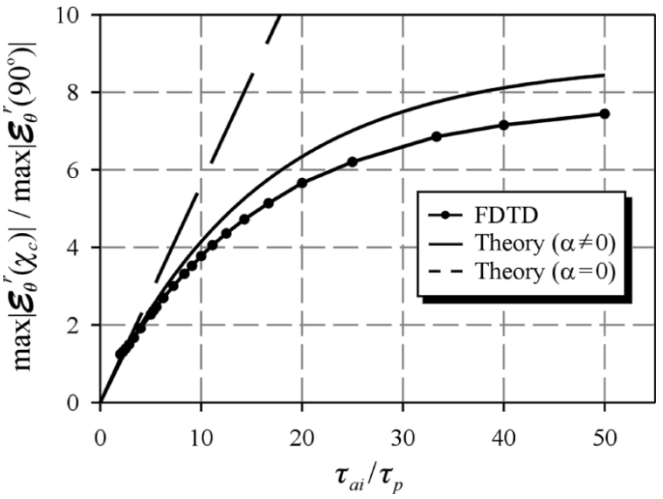

Fig. 13. Amplitude of the maximum electric field at the Cherenkov angle relative to that at broadside as a function of the normalized length of the antenna.

$\alpha c_{ni}\tau_p = 6.08 \cdot 10^{-2}$ (solid line), which was determined from the graphs of the charge distribution in Fig. 9, the ratio is seen to reach a plateau as the length of the antenna is increased, in close agreement with the FDTD results. Thus, increasing the length of the antenna increases the relative radiation at the analogous Cherenkov angle to a point, and beyond this point little additional radiation results from an increase in the length.

V. Conclusions

A realistic model for the pulse-excited, insulated traveling-wave antenna was accurately analyzed using the FDTD method. Graphical results were presented for the charge on the center conductor, the near field, and the radiated field (far field) of this antenna. These results show that the radiation from this antenna is analogous to Cherenkov radiation from a moving charged particle. The field near the antenna is most intense along a conical surface that is similar to the Mach cone for the charge, and the electric field is directed predominantly along the surface of this cone as it is for the charge. In the far field, the radiation from the antenna is primarily at the analogous Cherenkov angle, just as the radiation from a charged particle moving over a path of finite length is at the Cherenkov angle.

Acknowledgment

The authors would like to thank Dr. J. G. Maloney for helpful discussions of the FDTD analysis.

References

[1] P. A. Cherenkov, "Visible radiation produced by electrons moving in a medium with velocities exceeding that of light," *Phys. Rev.*, vol. 52, pp. 378–379, Aug. 15, 1937.

[2] G. S. Smith, *An Introduction to Classical Electromagnetic Radiation*. Cambridge, U.K.: Cambridge Univ. Press, 1997, ch. 6, sec. 6.4.

[3] I. Frank and Ig. Tamm, "Coherent visible radiation of fast electrons passing through matter," *Dokl. Akad. Nauk SSSR*, vol. 14, pp. 109–114, 1937.

[4] Ig. Tamm, "Radiation emitted by uniformly moving electrons," *J. Phys.*, vol. 1, pp. 439–454, 1939.

[5] R. W. P. King and G. S. Smith, *Antennas in Matter: Fundamentals, Theory, and Applications*. Cambridge, MA: MIT Press, 1981.

[6] A. H. Gods and Y. Rahmat-Samii, "Electromagnetic properties of an insulated dipole antenna immersed in an arbitrary medium," *Proc. Inst. Elect. Eng.*, vol. 138, no. 6, pp. 497–503, 1991.

[7] G. S. Smith, "Cherenkov radiation from a charge of finite size or a bunch of charges," *Amer. J. Phys.*, vol. 61, no. 2, pp. 147–155, 1992.

[8] T. W. Hertel, "Pulse radiation from an insulated antenna: An analogue of Cherenkov radiation from a moving charge," M.S. thesis, Georgia Institute Technol., Atlanta, GA, 1998.

[9] A. Taflove, Ed., *Computational Electrodynamics: The Finite-Difference Time-Domain Method*. Norwood, MA: Artech House, 1995.

[10] J. G. Maloney and G. S. Smith, "Modeling of antennas," in *Advances in Computational Electrodynamics: The Finite-Difference Time-Domain Method*, A. Taflove, Ed. Norwood, MA: Artech House, 1998, ch. 7.

[11] J. G. Maloney, M. P. Kessler, and G. S. Smith, "Generalization of PML to cylindrical geometries," in *Proc. 13th Annu. Rev. Progress Appl. Computat. Electromagn.*, 1997, pp. 900–908.

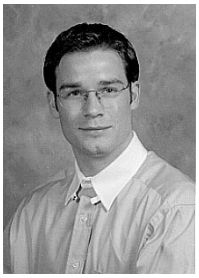

Thorsten W. Hertel (S'96) was born in Holzminden, Germany, on April 19, 1974. He received the Vordiplom in electrical engineering from the Technische Universitaet Braunschweig, Germany, in 1995, and the M.S.E.C.E. degree from the Georgia Institute of Technology, Atlanta, GA, in 1998. He is currently working toward the Ph.D. degree in electrical and computer engineering.

His special interests include numerical modeling with the finite-difference time-domain (FDTD) method and antenna analysis.

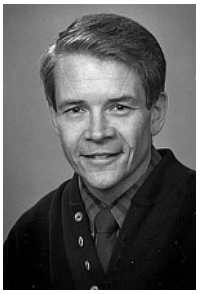

Glenn S. Smith (S'65–M'72–SM'80–F'86) received the B.S.E.E. degree from Tufts University, Medford, MA, in 1967, and the S.M. and Ph.D. degrees in applied physics from Harvard University, Cambridge, MA, in 1968 and 1972, respectively.

From 1972 to 1975, he served as a Postdoctoral Research Fellow at Harvard University and as a part-time Research Associate and Instructor at Northeastern University, Boston, MA. In 1975 he joined the faculty of the School of Electrical and Computer Engineering at the Georgia Institute of Technology, Atlanta, GA, where he is currently a Regents' Professor and John Pippin Chair in Electromagnetics. He is the author of *An Introduction to Classical Electromagnetic Radiation*, (Cambridge, U.K.: Cambridge Univ. Press, 1997) and coauthor of *Antennas in Matter: Fundamentals, Theory and Applications*, (Cambridge, MA: MIT Press, 1981). He also authored the chapter "Loop Antennas" in *Antenna Engineering Handbook*, (New York: McGraw-Hill, 1993). His technical interests include basic electromagnetic theory and measurements, antennas and wave propagation in materials, and the radiation and reception of pulses by antennas.

Dr. Smith is a member of Tau Beta Pi, Eta Kappa Nu, and Sigma Xi, and a member of URSI Commissions A and B.